Coadsorption of Sulfate/Bisulfate Anions with Hg Cations during Hg Underpotential Deposition on Au(111): An in Situ X-ray Diffraction Study

Jun Li and Héctor D. Abruña*

Department of Chemistry, Cornell University, Ithaca, New York 14853

Received: June 20, 1996[⊗]

The first stage of mercury underpotential deposition on Au(111) electrodes in 0.10 M H_2SO_4 containing 1.0 mM Hg^{2+} has been studied by synchrotron X-ray scattering techniques including grazing incidence X-ray diffraction and specular crystal truncation rod measurements. An ordered coadsorbed structure of sulfate/bisulfate anions and Hg cations was found at potentials between the first and second Hg UPD peaks ($+0.80$ V $\leq E \leq +0.88$ V vs Ag/AgCl(3 M KCl)). The coadsorption structure was found to consist of a compressed Hg honeycomb lattice with the honeycomb centers occupied by sulfate or bisulfate anions. The compression of the lattice is likely due to the formation of mercurous (Hg_2^{2+}) ions which have a much shorter Hg−Hg distance than that in frozen bulk Hg crystals. The net charge transferred under the first Hg UPD peak suggests that the chemical state of the species in the coadsorbed structure is likely Hg_2SO_4. Our results indicate that both the chemical state of the mercury cations and the nature of the anions are important in the resulting electrodeposited structures.

1. Introduction

The underpotential deposition (UPD) of metals onto foreign metal substrates has long been employed as model systems to understand the initial steps of electrodeposition within the submonolayer regime. It is now well established that this process involves not only adatom/substrate interactions, but also a strong interaction of deposited atoms with coadsorbed anions.[1−6] To understand these systems, at a microscopic level, it is important to know the detailed atomic structure of both metal atoms and anions on the substrate surface. In recent years, in situ microscopic techniques including scanning tunneling microscopy (STM),[7] atomic force microscopy (AFM),[8] and synchrotron radiation based surface X-ray scattering[9−11] have been successfully applied to UPD systems and have revealed complex atomic structures of metal atoms, anions, and their coadsorption at electrochemical interfaces. These studies have provided significant insights to numerous electrochemical processes such as adsorption, charge transfer, nucleation and growth, and electrocatalysis.

We report on an in situ surface X-ray scattering study of the coadsorption of sulfate (SO_4^{2-}) or bisulfate (HSO_4^-) anions with Hg cations during the UPD of Hg on Au(111) electrodes. There have been extensive studies of Hg electrodeposition on Au, especially polycrystalline surfaces, by conventional voltammetric methods.[12−16] It appears that mercury deposition on polycrystalline gold electrodes involves a two-stage process, with the first giving rise to a Hg(I) species (likely Hg_2^{2+}) with its subsequent reduction to metallic mercury. On single crystal Au(111) electrodes, monolayer deposition appears to also take place in two stages followed by bulk deposition. It has also been found that the mercury overlayer is stable in the UPD regime (i.e., at submonolayer coverage). Once the coverage exceeds one monolayer, the Hg atoms appear to diffuse into the bulk Au crystal to form an amalgam. However, this process is not well understood because of the lack of detailed microscopic structural information.

There have been AFM and STM studies geared at an understanding of the atomic structures of Hg UPD overlayers on Au(111). Using AFM, Gewirth and co-worker[17] investigated the structure of UPD Hg overlayers on Au(111) in four different supporting electrolytes and revealed a strong dependence of the Hg overlayer structure on the nature of the anion. They found that, in sulfate, nitrate, and perchlorate electrolytes, and at potentials just prior to bulk deposition, the overlayer presented a hexagonal structure with a lattice constant $a = 5.8 \pm 0.2$ Å. At potentials just after bulk deposition, they found a hexagonal lattice with an atom−atom spacing of $a = 2.9 \pm 0.3$ Å. On the other hand, both the feature and peak positions changed dramatically in acetate media. At potentials positive of the first UPD peak, the Hg overlayer presented a much larger hexagonal lattice with $a = 7.4 \pm 0.5$ Å. At potentials just prior to bulk deposition, the structure adopted a closed packed hexagonal lattice with $a = 3.1 \pm 0.2$ Å. Interestingly, at intermediate potentials, they identified an additional structure with a rhombic lattice with $a = 4.3 \pm 0.2$ Å and $\alpha = 81 \pm 3°$.

However, the results of Gewirth et al. are at odds with recent in situ STM studies of Itaya and co-workers[18] who found that the structure of the Hg adlayer in sulfuric acid is different from that in perchloric acid. In both cases, the Hg overlayers presented commensurate rectangular lattices which are different from the hexagonal lattices reported by Gewirth. Although there is a clear discrepancy in these results, they both indicate a strong effect of the supporting electrolyte anions on the resulting Hg UPD structures. It is also clear that mercury appears to form ordered adlayers when the deposition is within the monolayer regime. The ambiguity in the specific Hg adlayer structure may actually be due to anions adsorbed on top of the Hg adlayer since both AFM and STM are most sensitive to the topmost surface.

On the other hand, synchrotron radiation based surface X-ray diffraction has the advantage, over scanning probe microscopy techniques such as STM and AFM, in that it is not invasive and X-ray photons can penetrate down to the bulk substrate. Thus, surface X-ray scattering measurements can provide multilayer structural information along the surface normal as well as the atomic arrangement within the surface plane. This is particularly valuable for the study of anion coadsorption during UPD processes which involve multilayers or multicomponents in the structure.

[⊗] Abstract published in *Advance ACS Abstracts,* December 15, 1996.

S1089-5647(96)01857-3 CCC: $14.00

The use of in situ surface X-ray scattering techniques to the study of UPD processes is now well established. Toney and co-workers recently reported on a study of the UPD of Cu on a Au(111) electrode in sulfuric acid media.[19] They found a honeycomb lattice of Cu atoms (2/3 monolayer (ML) coverage) with sulfate anions adsorbed in the centers (1/3 ML coverage) and above the plane of Cu atoms. Three oxygen atoms of each sulfate molecule are chemically bonded to Cu atoms, and the other one points away from the surface. This structure, first proposed by Blum and co-worker,[20] explains most of the large body of data that exists for this system and provides a much deeper understanding of the stabilization of this structure.

However, there is still some controversy as to the structure of sulfate/bisulfate itself on Au(111) in the absence of an underpotentially deposited metal overlayer. There have already been extensive STM,[21,22] FTIR,[22] chronocoulometry,[23] and radiochemical[23] studies on this system. The cyclic voltammogram of Au(111) in 0.10 M H_2SO_4 shows a sharp peak at +0.83 V (vs Ag/AgCl (3 M KCl)) ostensibly corresponding to the formation of an ordered sulfate/bisulfate overlayer. Using in situ STM, Magnussen et al.[21] found that, at potentials above this peak, the adsorbed anions form a centered $\sqrt{3} \times \sqrt{7}$ structure with a surface coverage of 0.4 ML. At potentials below this value, only the (1×1) Au(111) surface structure is observed. From the absence of this structure in Na_2SO_4 solution, they concluded that the adsorbed species is likely bisulfate instead of sulfate. However, based on a quantitative thermodynamic analysis of chronocoulometric measurements, Shi et al.[23] concluded that sulfate rather than bisulfate was the predominant adsorbate, even in strongly acidic (pH $\approx$ 1) solutions, and that the surface coverage is about 0.2 at the potential where the ordered overlayer should be formed. Edens et al.[22] observed an STM image similar to that reported by Magnussen et al., but they interpreted the image with a model consisting of adsorbed sulfate at a coverage of 0.2 (instead of 0.4), which is in agreement with Shi's results. Extra satellite STM spots were attributed to hydronium cations which coadsorbed with the sulfate anions. Recently, Itaya and co-workers[18] found a similar STM image of sulfate on Au(111) in 0.05 M H_2SO_4 containing 1.0 mM Hg^{2+} at a potential ($\sim$+1.05 V) prior to the first Hg UPD (at +0.93 V vs Ag/AgCl (3 M KCl)). They proposed a model with hydrogen-bonded water chains incorporated between the $\sqrt{3} \times \sqrt{7}$ anion rows. They suggest that there are two water molecules per sulfate anion and one of them is protonated to form a hydronium cation. However, the net charge transferred to the surface by the adsorption of a SO_4^{2-} anion and a hydronium cation is equivalent to the adsorption of a HSO_4^- anion, which is not fully consistent with chronocoulometric data. There is still a lack of consensus among all these experimental results, and additional data from other surface structure sensitive techniques, such as X-ray scattering, may help clarify the detailed structure.

In this paper, we report on the study of sulfate/bisulfate anions coadsorbed during Hg UPD on a Au(111) electrode by the combination of grazing incidence X-ray diffraction (GIXD) and specular crystal truncation rod (CTR) measurements. GIXD provides information on the in-plane atomic arrangement,[24] while CTR reveals the electron density profile in the direction normal to the surface.[25] The paper is organized as follows. The experimental details (section 2) and detailed electrochemical behavior of Hg UPD on Au(111) electrodes (section 3.1) are described first. CTR measurements of Au(111) in 0.10 M H_2SO_4 at various electrode potentials will be discussed next (in section 3.2) and serve as a reference to the structure of the sulfate/bisulfate adlayer on Au(111) electrodes prior to Hg UPD. In section 3.3, the GIXD data are presented and a real space lattice is directly derived from the diffraction spots in reciprocal space. The CTR data at potentials where ordered coadsorption is observed are discussed in section 3.4. Analysis of these data reveals that the coadsorption structure consists of two layers. In section 4, we combine all the experimental results and propose a detailed structure which is compared with previous studies of Cu UPD on Au(111) electrodes. Finally, conclusions are presented in section 5.

2. Experimental Section

Au(111) single crystals were used in both cyclic voltammetric studies and X-ray diffraction measurements. The crystals ($\sim$9 mm in diameter and 2 mm thick) were grown from the melt at the materials preparation facility of Cornell University. They were first oriented by X-ray diffraction along the (111) direction to ensure that the miscut angles were less than 0.3°. Each crystal was then successively polished with various sandpapers, diamond pastes, and alumina powders with the finest grain diameter down to 0.05 μm. Following the mechanical polish, the crystal surface was chemically etched with a solution of KI and I_2 to eliminate the top layer damaged during the polishing procedure. Each new crystal used in our studies was treated in an UHV chamber by argon ion bombardment and long time annealing at a temperature of $\sim$800 °C. This process was repeated several times until the surface was found to be free of impurities, as indicted by Auger electron spectroscopy in addition to showing a sharp $p \times \sqrt{3}$ reconstruction by LEED. After this procedure, high quality single crystals were obtained with coherence lengths typically on the order of thousands of angstroms. In subsequent experiments, a flame annealing method was employed to prepare a fresh clean surface just prior to use. The crystal was annealed for about 5 min with a propane torch in air at a temperature where the crystal starts to turn from red to white (approximately 900 °C). After cooling in air for about 1 min, a drop of ultrapure deionized water was placed onto the surface to protect it from contaminants. The crystal was then quickly transferred into the X-ray scattering cell and submerged in the electrolyte solution previously bubbled with ultrapure nitrogen. In cases when the surface was contaminated or damaged (e.g., due to bulk deposition of Hg), the chemical etching procedure with the KI and I_2 mixture was repeated so as to recover the high quality sample.

In electrochemical studies, a similar electrode pretreatment was used, and contact to just the (111) face was achieved by the hanging meniscus method. In both cyclic voltammograms and surface X-ray diffraction experiments, a Ag/AgCl (3 M KCl) reference electrode was used without regard for the liquid junction. A large area coiled platinum wire was used as a counter electrode. High purity H_2SO_4 (Ultrex, J. T. Baker) and ultrapure water (Milli-Q water or Barnstead) were used to make solutions. Solutions containing Hg^{2+} were prepared by dissolving HgO (Alfa, 99.998%) into appropriate solutions. Electrochemical experiments were carried out with a BAS CV-27 potentiostat and recorded with a BAS X-Y recorder. In some cases, a PAR 283 potentiostat interfaced with Corrware software was employed.

X-ray diffraction experiments were performed at the Exxon X10B beamline at the National Synchrotron Light Source using a four circle diffractometer. On this beamline, the synchrotron radiation from the bending magnet of the electron storage ring is focused with a Pt-coated bent cylindrical mirror and monochromatized with a single Si(111) crystal. X-ray photons of 1.1287 Å wavelength were employed. The sample cell has a reflection geometry and is similar to those used in previous

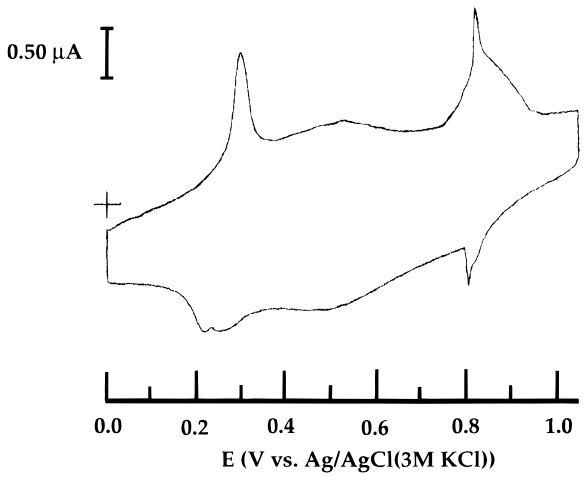

Figure 1. Cyclic voltammogram of a Au(111) electrode in 0.10 M sulfuric acid at a scan rate of 10 mV/s.

studies.[26,27] X-ray photons penetrate through a 2.5 μm Mylar film (Chemplex) as well as a thin film of electrolyte (estimated to be about 30 μm) covering the Au(111) crystal. To prevent the diffusion of oxygen from air through the Mylar film, an outer shield with a Kapton window (Chemplex) was placed on top of the sample cell and continuously flushed with ultrapure N_2. Cyclic voltammograms in the X-ray cell were carried out with the Mylar film inflated by additional electrolyte solution. For X-ray measurements, electrolyte was withdrawn to achieve a thin layer configuration. Each time the electrode potential was changed to a new value, the Mylar film was again inflated by adding more deoxygenated electrolyte and held in this condition for about 5 min to ensure equilibration. Only in specified cases, X-ray scattering measurements were taken with the Mylar film pressed down while scanning the electrode potential so as to follow, in real time, the change in scattered intensity.

The X-ray reflections are referred to the hexagonal coordinates of the Au(111) substrate with $\mathbf{a}_s$ and $\mathbf{b}_s$ along the nearest-neighbor direction in the surface plane ($a_s = b_s = 2.885$ Å) and $\mathbf{c}_s$ ($c_s = 2.3556$ Å) normal to the surface. The **Q** vectors are described by two components with $Q_{||}$ in the surface plane and Q_z along the surface normal. GIXD measurements were carried out in the azimuth fixed mode where the incident and outgoing angles were kept small ($\alpha = \beta \approx 3.5°$, $L = 0.1$ reciprocal lattice units (rlu)) so as to reduce the background and absorption by the Mylar film and water solution. A complete CTR measurement consists of a series of surface rocking curves at Q_z from 0 to 2 rlu. Each of these rocking curves was fitted to a Lorentzian line shape to derive the integrated intensity, which was subsequently used for fitting with a model consisting of atomic layers along the surface normal.

3. Results

3.1. Cyclic Voltammetry. As a point of departure, we carried out voltammetric measurements for the Au(111) electrode in both 0.10 M H_2SO_4 solution and 0.10 M H_2SO_4 solution containing 1.0 mM Hg^{2+}. Figure 1 shows a cyclic voltammogram of Au(111) in 0.10 M H_2SO_4 at a scan rate of 10 mV/s covering the double-layer region. It presents features similar to those reported previously.[21] The peak at +0.30 and the broad peak between +0.30 and +0.80 V are ascribed to a structural transition of the originally reconstructed Au(111) surface into the unreconstructed (1 × 1) phase due to the adsorption of anions onto the surface. The sharp peak at +0.83 V is attributed to a transition of the adsorbed anions to an ordered structure.

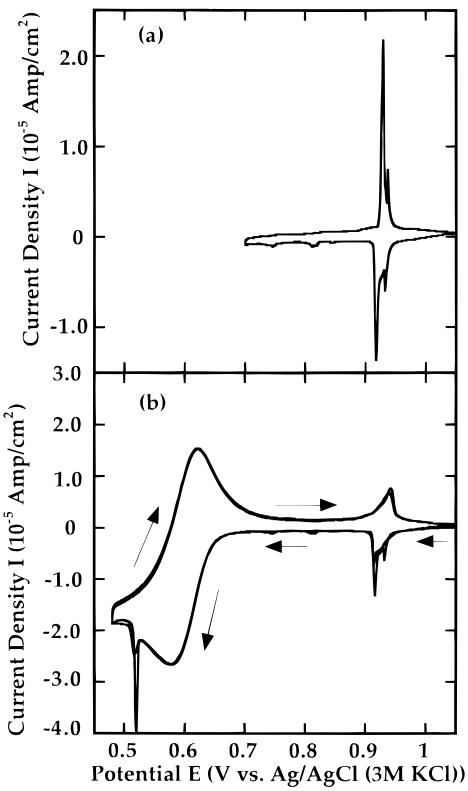

Figure 2. Cyclic voltammogram of a Au(111) electrode in 0.10 M sulfuric acid containing 1 mM Hg^{2+} at a scan rate of 2 mV/s, where the potential is scanned (a) between +0.70 and +1.05 V vs Ag/AgCl (3 M KCl) and (b) between +0.48 and +1.05 V. The arrows in (b) indicate a scan initiated at +1.05 V in the negative direction and then reversed at $E = +0.48$ V.

The electrochemical behavior is dramatically changed when Hg^{2+} ions are introduced into the solution as shown in Figure 2 for a Au(111) electrode in 0.10 M H_2SO_4 solution containing 1.0 mM Hg^{2+}. In Figure 2(a), where the potential is cycled between +0.70 and +1.05 V, there are two sets of very sharp peaks around +0.93 V. There are also two additional weak and broad peaks centered at +0.77 and +0.84 V, respectively. These features are similar to those reported before by Itaya and co-workers[18] and are very reproducible without any change in the shape or height for several hours of scanning within this potential range. This indicates that the substrate surface is stable to long term scanning and that no amalgam is formed within this potential range. The net charge derived from the integration of the double peaks around +0.93 V is found to be 98 ± 10 μC cm^{-2}. An ideal Au(111) surface would have 444 μC cm^{-2} of charge if there were two electrons transferred per Au atom. Assuming that only Hg atoms are deposited onto the surface and that they are present as Hg(0), the surface coverage of Hg (i.e., the Hg to Au atomic ratio) is calculated to be 0.21. However, since the electrodeposition process likely involves the coadsorption of sulfate/bisulfate anions, this number needs to be considered with caution and in light of other experimental results, as will be discussed later.

When the electrode potential is scanned to more negative values, additional redox processes are observed. As shown in Figure 2(b), the first cathodic scan which starts at +1.05 V shows all the reduction features mentioned earlier. Upon further scanning of the potential to +0.60 V, a broad and diffusional-like reduction peak is apparent. Interestingly, there is a very sharp spike at +0.52 V superimposed on the broad reduction wave. There is no corresponding sharp oxidation peak if the scan direction is reversed into the positive direction after this spike. Instead, only a broad oxidation peak corresponding to

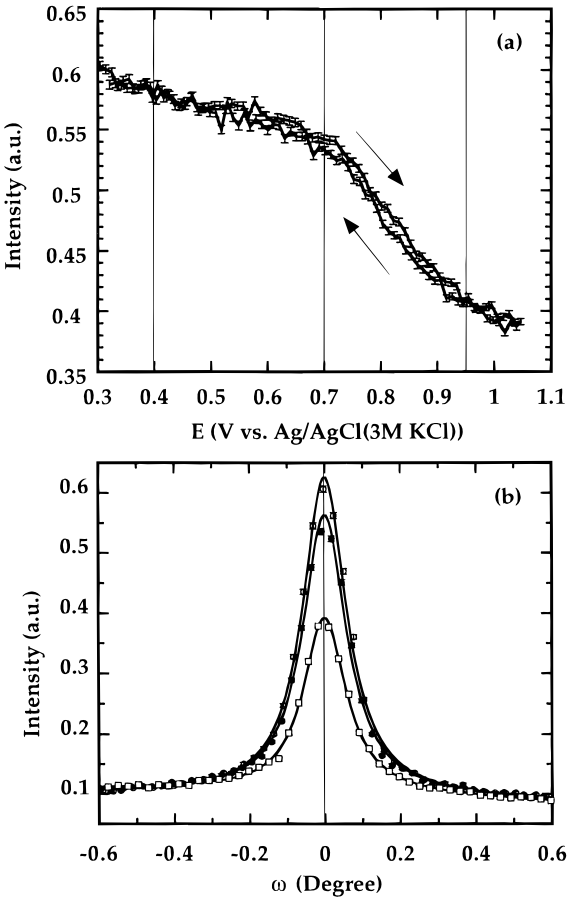

Figure 3. (a) Intensity change at (0, 0, 0.5) while scanning the electrode potential at 1 mV/s. The arrows indicate the direction of the scan. (b) Rocking curves of (0, 0, 0.5) at $E = +0.40$ V (open squares), $+0.75$ V (filled circles), and $+0.95$ V (open circles). The thin vertical lines in (a) indicate the potentials at which the rocking curves in (b) were measured. The continuous lines in (b) are the fits with Lorentzian shapes.

the broad reduction peak mentioned above appears. Moreover, once the electrode potential is scanned negative of this sharp spike, the sharp double peaks at $+0.93$ V were dramatically broadened and appear as a single peak in successive scans. However, if the scan direction is reversed right on the sharp spike at $+0.52$ V, a sharp oxidation spike also appears on the subsequent anodic sweep (not shown) and the changes in the double peaks at $+0.93$ V are greatly minimized. The broad peak at $+0.60$ V likely corresponds to the deposition of the first Hg monolayer, and the sharp spike at $+0.52$ V indicates the completion of this monolayer and the onset of amalgam formation. We focus here on describing the microscopic processes corresponding to the first stage of Hg UPD occurring at $+0.70$ V $< E < +1.0$ V. The structure of the Hg UPD layer at $E < +0.70$ V will be addressed elsewhere.[28]

3.2. Anion Adsorption in 0.1 M H_2SO_4 Solution: CTR Results. In order to better understand the structure of the coadsorbed anions during Hg UPD on a Au(111) surface, we first studied the adsorption of sulfate/bisulfate anions on bare Au(111) electrodes in pure 0.10 M H_2SO_4.

When a surface is covered with an overlayer, the electron density profile along the surface normal will be different from that of an ideally truncated surface. The scattered intensity at the anti-Bragg points of the specular CTR such as (0, 0, 0.5) is very sensitive to such changes and can be used to reveal details of the adsorption and desorption processes. Figure 3a shows the potential dependence of the peak intensity at (0, 0, 0.5) for a Au(111) electrode in 0.10 M H_2SO_4 solution during a potential

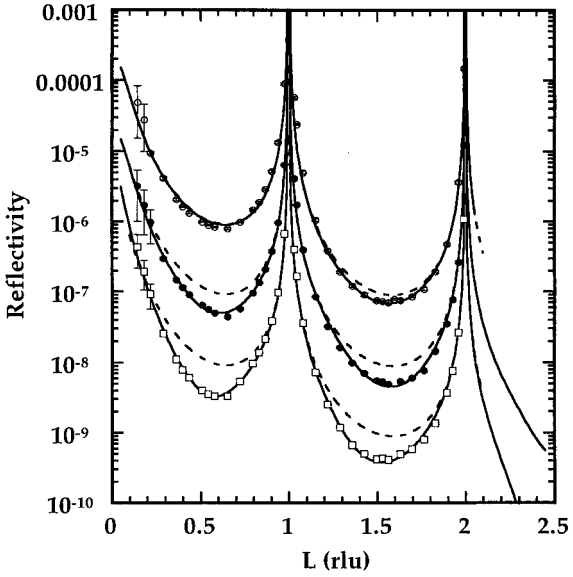

Figure 4. CTR data at $E = +0.40$ V (open circles), $+0.75$ V (filled circles), and $+0.95$ V (open squares). The data at $E = +0.75$ V and $E = +0.95$ V are shifted by 1 and 2 orders of magnitude, respectively, to give a better view. The dashed lines are the calculation of the CTR of an ideally truncated Au(111) surface, and the continuous lines are the fits with a multilayer model (see text).

scan at a rate of 1 mV/s. During this measurement, the Mylar film was pressed down on the crystal surface so that the scattered intensity changes could be followed in real time. The adsorption/desorption processes were found to be rapid in this system, and no diffusional hindrance was observed.

As can be seen in Figure 3a, at potentials below $+0.70$ V, there are only small changes in intensity. However, over the range from $+0.70$ to $+0.95$ V, the intensity drops significantly and reaches a plateau at potentials above $+0.95$ V. Qualitatively, the intensity profile indicates that an adsorbate overlayer starts to form on the electrode surface at $E = +0.70$ V and is completed at $E = +0.95$ V. The fact that no hysteresis is observed in the reverse scan (Figure 3(a) shows one full scan) indicates that the adsorption/desorption processes are quite reversible, which is in good agreement with STM results.[21]

Quantitative analysis of specular CTR data requires the integration of the intensity of rocking curves at a series of Q_z values over several Bragg points in (00L). We took complete CTR measurements at three representative potentials: $+0.40$, $+0.70$, and $+0.95$ V, respectively, as indicated by the vertical lines in Figure 3(a). Typical rocking curves of (0, 0, 0.5) at these three potentials are shown in Figure 3(b) with the corresponding Lorentzian fits (continuous lines). It is clear from the figure that the peak amplitude decreases significantly as the potential is changed from $+0.40$ to $+0.95$ V. The background intensity at all three potentials is virtually constant since it is mainly due to scattering from the Mylar film and the thin layer of electrolyte solution covering the crystal.

Figure 4 shows the complete CTR profiles measured at $E = +0.40$ V (open circles), $+0.70$ V (filled circles), and $+0.95$ V (open squares), respectively. The vertical axis is plotted on a logarithmic scale to cover the large dynamic range of the X-ray specular reflectivity. The data sets at $E = +0.70$ and $+0.95$ V are shifted down by a factor of 10 and 100, respectively, to give a clearer view. The dashed lines are the calculated values for an ideally truncated Au(111) crystal, and the continuous lines are the fitted CTR curves. As can be ascertained, at an applied potential of $+0.40$ V, the fitting line at $E = +0.40$ V is almost superimposed on the ideal Au(111) CTR curve, suggesting an ideal termination of the crystal with little adsorbed species. At

TABLE 1: Specular CTR Fitting Parameters at Different Potentials

E (V)	adsorbate species	ρ_0	σ_0 (Å)	d_0 (Å)	ρ_1	σ_1 (Å)	d_1 (Å)
+0.40		1	0.127 ± 0.014	2.362 ± 0.009			
+0.70	H_2O	1	0.143 ± 0.015	2.355 ± 0.006	1.19 ± 0.11	0.2	2.13 ± 0.1
+0.70	SO_4^{2-}/HSO_4^-	1	0.144 ± 0.022	2.358 ± 0.008	0.247 ± 0.022	0.2	2.11 ± 0.12
+0.95	SO_4^{2-}	1	0.169 ± 0.019	2.388 ± 0.006	0.4 ± 0.025	0.2	2.127 ± 0.055

+0.70 and +0.95 V, the intensity at the valleys becomes deeper and deviates significantly from the ideal curves.

The specular CTR curve of a Au(111) crystal covered with an overlayer can be calculated as a simple sum over the scattering from atomic layers with Gaussian electron density profiles as described in previous studies.[27] Similar to the method used before, each atomic layer is described by three parameters: the coverage or density ρ_m (defined as the atomic ratio of the species in the mth layer to that of Au in a Au(111) layer), the Gaussian width σ_m (defined as the root mean square displacement of the species in the layer), and the distance d_m to the next lower layer.[29] The atomic scattering factors were numerically calculated from the empirical equations in the International Tables for Crystallography.[30] For an ideal Au(111) crystal, the parameter for each bulk atomic layer is defined as $\rho = 1$, $\sigma = 0.085$ Å, and $d = 2.3556$ Å.[31] However, the topmost layer is typically slightly different from that of the bulk layer. The parameters for the topmost Au(111) layer (σ_0 and d_0) and those for the successive adsorbate layers (ρ_m, σ_m, and d_m with $m = 1, 2, ...$) were left free to change during fitting.

The fitted parameters at different potentials are listed in Table 1. At $E = +0.40$ V, the Au(111) surface appears to be, within the detection limit of the experiment, free of any adsorbate. This is reasonable since the potential of zero charge (E_{pzc}) of Au(111) electrodes in 0.10 M sulfuric acid is estimated to be about +0.30 V.[32] The top layer density ρ_0 is fixed at 1 during fitting because the surface is known to present a (1 × 1) structure and the size of the atomically flat terraces on the surface is larger than that of the coherence length of the incident photons. The distance between the topmost and the second Au(111) layer was found to be identical to that of the bulk crystal. However, the root mean square (rms) displacement of the topmost Au(111) layer (0.127 ± 0.014 Å) was larger than that of the bulk value (0.085 Å). This is typical for surface layers, particularly for surfaces in contact with electrolyte solutions.

At $E = +0.75$ V, two models were attempted in fitting the experimental data. In the first one, the Au(111) surface was assumed to be covered with a layer of water. The fitted surface coverage was found to be 1.19 ± 0.11. The second model consisted of a sulfate/bisulfate overlayer instead of adsorbed water molecules. The coverage obtained was 0.247 ± 0.022 so that the total electron density in the overlayer was the same as that of a layer of water. In both cases, the overlayer to Au(111) distance was found to be virtually identical with values of 2.13 ± 0.1 and 2.11 ± 0.12 Å, respectively. The rms displacement (σ_1) of the adsorbate was fixed at 0.2 Å because the CTR curve is not particularly sensitive to it. Changing σ_1 from 0.2 to 0.35 Å resulted in only a slight increase in the water coverage ρ_1 from 1.19 to 1.23 with the same overall fitting quality. The topmost Au(111) layer is almost identical to that of the "clean" surface at $E = +0.40$ V with only a slight increase in σ_0 from 0.127 ± 0.014 to 0.143 ± 0.015 Å. This would suggest that the adsorbate is likely water molecules rather than the sulfate/bisulfate which has a stronger interaction with the Au surface. However, the slope change at $E = +0.70$ V (as shown in Figure 3(a)) might suggest that a full monolayer of water is probably completed around this potential and water molecules start to be replaced by sulfate/bisulfate anions as the potential is made progressively more positive.

Finally, a full monolayer of sulfate/bisulfate appears to be formed at $E \geq +0.95$ V. The topmost Au(111) surface exhibits a larger rms displacement $\sigma_0 = 0.169 \pm 0.019$ Å and a larger interlayer distance $d_0 = 2.388 \pm 0.006$ Å when compared to values at lower potentials. The surface coverage ρ_1 of the sulfate/bisulfate anions was found to be 0.4 ± 0.025 at a distance $d_1 = 2.127 \pm 0.055$ Å from the substrate surface. This coverage is consistent with the model proposed by Magnussen et al. as previously mentioned.[21] On the other hand, Itaya's model[18] would yield an overlayer density equivalent to a sulfate layer with $\rho_1 = 0.28$ which is clearly well beyond the error bar of the fitting value. However, additional water molecules could be incorporated into the overlayer to form a more complicated structure. Based on CTR data alone, we cannot conclusively exclude Itaya's model.

In principle, a detailed model could be determined by a combination of CTR and GIXD measurements. However, we were unable to find any in-plane X-ray diffraction in sulfuric acid solutions even though highly ordered adsorbate structures have been observed by STM as mentioned earlier. This might be due to the incoherent arrangement of oxygen atoms in the overlayer. The X-ray scattering from sulfur atoms alone is too weak to be detected due to the rather high background intensity present in in situ experiments. However, the agreement of our X-ray CTR results with some previous studies is valuable in providing a base for further studies of the anion coadsorption during Hg UPD.

3.3. Ordered Coadsorbed Adlayer during Hg UPD: GIXD Results. As mentioned before, the $\sqrt{3} \times \sqrt{7}$ sulfate adlayer has also been observed by STM in sulfuric acid solutions containing Hg^{2+} ions at potentials prior to the first Hg UPD peak ($E > +0.93$ V). The Hg^{2+} ions appear to stabilize this long-range-ordered structure.[18] Our CTR data in 0.10 M H_2SO_4 with 1.0 mM Hg^{2+} at $E > +0.93$ V are identical to those in pure sulfuric acid solutions. We were thus encouraged to investigate whether the Hg^{2+} ions might help form an ordered sulfate/bisulfate overlayer. However, we were unable to observe any in-plane diffraction at these potentials.

Nonetheless, when the potential was changed to a value lower than the first UPD peak, we found a highly ordered new structure within the rather narrow potential range of $+0.80$ V $\leq E \leq +0.88$ V. The observed peak positions of in-plane diffraction from a single domain of a Hg overlayer are plotted overlaid on the reciprocal space map of a Au(111) surface as shown in Figure 5(a). The index $(h,k)_a$ refers to diffraction from the overlayer and $(h,k)_s$ refers to diffraction from the Au(111) substrate. All measurements were taken at $L = 0.1$ rlu at a grazing incidence angle. Peaks at $(1,0)_a$, $(2,0)_a$, $(0,1)_a$, and $(1,1)_a$ unambiguously define the reciprocal unit cell of the overlayer. Clearly, the overlayer has an oblique unit cell with one vector aligned in the next-nearest-neighbor direction of the Au(111) surface. The overlayer diffraction spot $(1,0)_a$ can be also indexed with the substrate notation as $(0.75,-0.375)_s$ which is along the higher order diffraction of Au(111) at $(2,-1)_s$.

The real space structure can be directly derived from the size and geometry of the reciprocal lattice and is shown in Figure 5(b). The open circles at the bottom represent Au atoms and the filled circles represent overlayer unit cell points instead of atoms. The primitive cell has lattice parameters $a = 4.197 \pm$

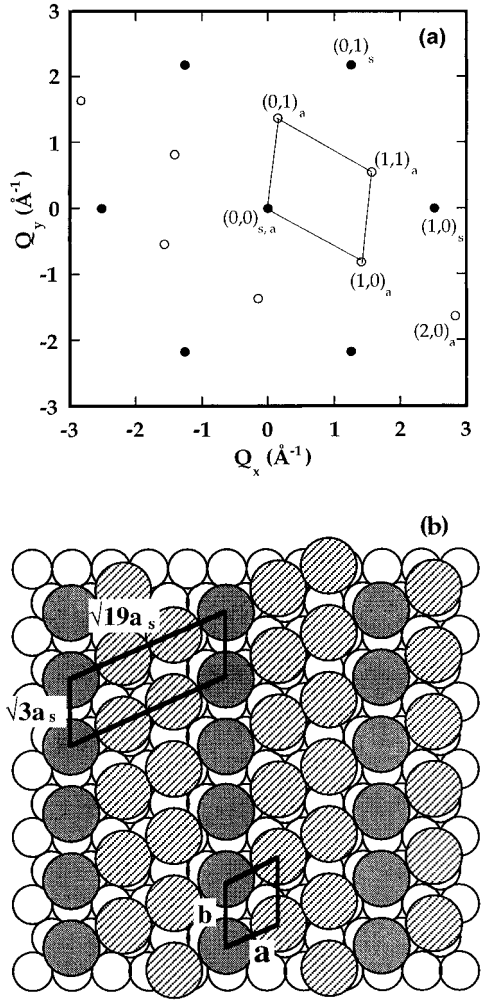

Figure 5. (a) Reciprocal space map of the in-plane diffraction of the coadsorption structure (open circles) relative to that of Au(111) surface (filled circles). (b) Real space lattice directly derived from the reciprocal lattice in (a). The open circles represent the Au(111) surface atoms, and the dark circles represent the overlayer units assumed at the 3-fold hollow sites of Au(111). The hatched circles represent other overlayer units.

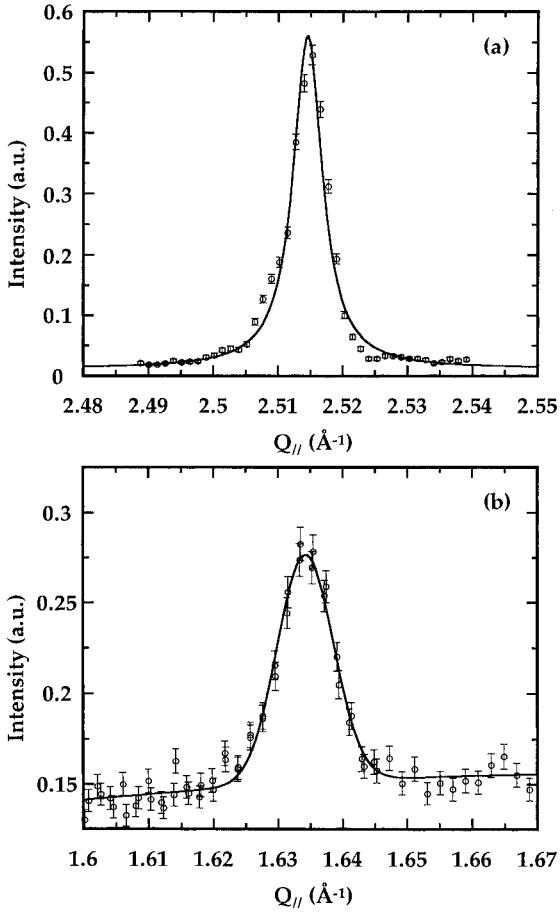

Figure 6. In-plane radial scan (open circles) across (a) the Au(111) surface peak $(1,0)_s$ and (b) the coadsorption structure. The Au(111) surface peak is fitted by a Lorentzian while the coadsorption peak is better fitted with a Gaussian.

0.0026 Å, $b = 4.996 \pm 0.0036$ Å, and $\alpha = 66.3°$. Interestingly, the lattice parameter b is exactly $\sqrt{3}a_s$ and along the diagonal direction of the Au(111) lattice. Thus, it forms commensurate rows (dark circles) along the **b** axis. The commensurate rows repeat along **a** every three units and form a larger commensurate cell which can be described as $\sqrt{3} \times \sqrt{19}$. The $\sqrt{3} \times \sqrt{19}$ cell is consistent with one of Itaya's STM images[18] of Hg UPD on Au(111) at the same potential. However, Itaya and co-workers proposed a model with only two adsorbate units in the $\sqrt{3} \times \sqrt{19}$ cell while our X-ray data indicates three adsorbate units in each cell. This discrepancy might be again due to the instability of coadsorbed anions. Interestingly, the previously mentioned $\sqrt{3} \times \sqrt{7}$ structure of sulfate is also only slightly different from a superlattice of the primitive oblique cell in both size and geometry. The fact that we observe the primitive oblique cell instead of the $\sqrt{3} \times \sqrt{19}$ superlattice cell by GIXD indicates that the in-plane diffraction is rather insensitive to the difference in adsorbate sites in this case. The information of the detailed adsorbate sites can be derived, in principle, from nonspecular CTR measurements which are to be discussed elsewhere.[33] The area per primitive cell is 19.20 Å^2 which gives a surface coverage of 0.375 which is only slightly smaller than the value of 0.4 in Magnussen's model.

The in-plane radial scans across the substrate diffraction $(1,0)_s$ and overlayer diffraction $(1,0)_a$ are shown in Figure 6, panels (a) and (b), respectively. The Au(111) diffraction is better fitted by a Lorentzian rather than a Gaussian distribution. It gives a line width of 0.00549 ± 0.00036 Å^{-1} which is limited by the detector slit. However, it confirms that the coherence length of the Au(111) surface is larger than 1144 ± 40 Å. On the other hand, the scan of the overlayer can be fitted with the same quality by either a Lorentzian or a Gaussian. The width fitted by a Gaussian is 0.0102 ± 0.00036 Å^{-1}, which corresponds to a coherence length of 615 ± 22 Å. This rather large coherence length indicates the high long-range order in the overlayer, which is the reason that we observe a rather strong second order diffraction signal at $(2,0)_a$.

3.4. Two-Layer Coadsorption Structure: CTR Results. The in-plane structure derived from GIXD measurements only reveals the lattice of adsorbates on the surface. More detailed understanding about the exact atomic arrangement in the unit cell requires other complementary information. In this section, we discuss specular CTR measurements which provide information along the surface normal.

Figure 7(a) shows the CTR data (filled circles) in 0.10 M H_2SO_4 solution containing 1.0 mM Hg^{2+} ions at $E = +0.80$ V, where we observed the in-plane diffraction from the adsorbed overlayer. It shows much deeper valleys around 0.5 and 1.5 rlu with intensities about 2 orders of magnitude lower than the curve for an ideally truncated Au(111) surface (dashed line). Interestingly, the experimental data show a clear asymmetric feature, indicating that the structure probably involves more than one layer.

The best fit is plotted as the continuous line in Figure 7(a). It nicely follows all the detailed features of the experimental

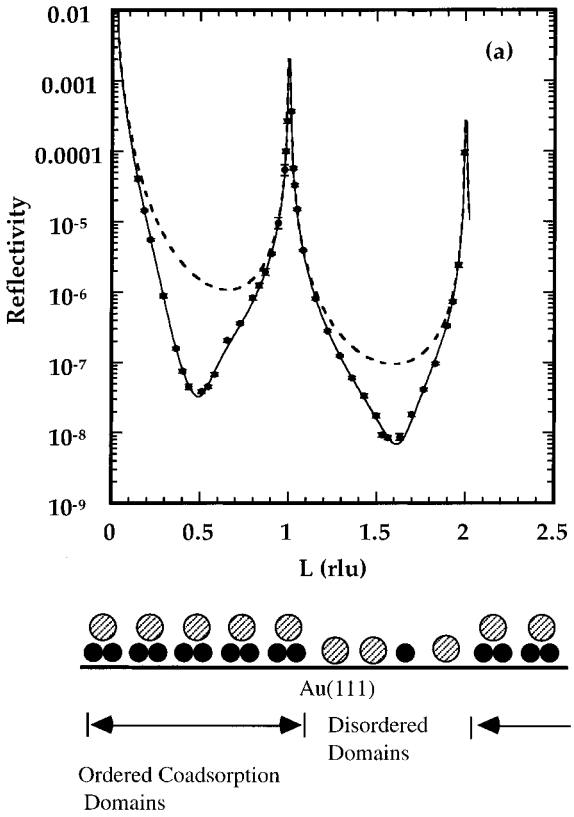

Figure 7. (a) CTR data of the Au(111) surface with the coadsorption overlayer. The dashed line is calculated for an ideally truncated Au(111) crystal, and the continuous line is the fit by the two-layer model. (b) Schematic depiction of the two-layer model.

data with an excellent fitting quality defined by $\chi^2 = 3.481$. The topmost Au(111) layer ($\rho_0 = 1$) shows a larger surface roughness ($\sigma_0 = 0.2162 \pm 0.0046$ Å) and a slightly smaller interlayer distance ($d_0 = 2.3125 \pm 0.0028$ Å) than on a surface covered with sulfate/bisulfate alone (see section 3.2). The adsorbate consists of two layers, as shown in Figure 7(b), with a mercury layer (filled circles) directly on top of the Au(111) surface and a sulfate/bisulfate layer (hatched circles) on top of the mercury. The mercury layer has parameters $\rho_1 = 0.616 \pm 0.012$, $\sigma_1 = 0.505 \pm 0.026$ Å, and $d_1 = 2.457 \pm 0.018$ Å, while the sulfate/bisulfate layer presents $\rho_2 = 0.254 \pm 0.041$, $\sigma_2 = 0.66 \pm 0.17$ Å, and $d_2 = 2.641 \pm 0.057$ Å. The mercury to Au(111) distance is only slightly larger (by ~0.1 Å) than that of the interlayer distance of the bulk Au(111) crystal. However, the fitted Hg coverage is much larger than the value of 0.375 calculated from the in-plane structure. Therefore, the unit cell in Figure 5(b) must consist of more than one atom. Moreover, the ratio of Hg to sulfate/bisulfate has a rather peculiar value of 2.43. It is not clear, at this moment, what the exact interfacial composition is.

As mentioned in the last section, the coherence length of the overlayer is less than that of the Au(111) surface. Thus, the ordered overlayer domains are likely present as islands on the surface. Between the ordered domains, the bare Au(111) surface could be covered by either a monolayer of sulfate/bisulfate anions or disordered Hg atoms. A possible structure is schematically shown in Figure 7(b). The anions or Hg atoms directly deposited onto the bare Au(111) surface will increase the electron density in the first layer and make the fitted Hg coverage larger than the number in a perfectly ordered coadsorption domain.

We first assumed that the species directly adsorbed on the bare Au surface are sulfate/bisulfate anions and that they have the same density as that described in section 3.2. From the in-plane structure, we know that a fully covered ordered coadsorption domain will give a sulfate/bisulfate anion coverage of 0.375. However, the fitted coverage for the second anion overlayer is 0.254 ± 0.041. Therefore, the ordered coadsorption domains cover only $0.254/0.375 \approx 68\%$ of the Au(111) surface. The other 32% of the Au(111) surface is likely covered with a sulfate/bisulfate monolayer. In order to match the fitted density in the first layer, we have to assume that each coadsorption unit cell consists of two Hg atoms and one sulfate/bisulfate anion. Then the 68% ordered coadsorption domain gives an equivalent first-layer Hg coverage of $68\% \times 0.375 \times 2 = 0.51$. The anions on the 32% bare Au(111) surface given an equivalent first-layer Hg coverage of $32\% \times 0.4 \times 48/80 \approx 0.077$. The sum of these two terms gives 0.587, which is only slightly beyond the error of the fitted value of 0.616 ± 0.012. Therefore, there must be some disordered Hg atoms coadsorbed with anions in the 32% region. The inhomogeneous nature of this system makes it difficult to derive the exact composition in the disordered region. However, the model in which each unit cell of the ordered coadsorption structure consists of two Hg atoms and one sulfate/bisulfate anion agrees with our present data and explains the high intensity in our GIXD measurements.

4. Detailed Structure

As a summary, in previous sections, we showed evidence of a highly ordered structure of sulfate/bisulfate coadsorbed with Hg cations during Hg UPD. CTR measurements revealed that each unit cell consisted of two Hg atoms and one sulfate/bisulfate anion to form a bilayer structure. We now address the detailed structure of the coadsorbed layer.

This coadsorption structure is rather complicated because deposited Hg atoms are likely not fully discharged. In addition, it is still not clear whether sulfate or bisulfate is coadsorbed with Hg and how it affects the thermodynamics and kinetics of the deposition process. However, a similar coadsorption structure at the first stage of Cu UPD on Au(111) has been extensively studied by various techniques, and we can use these results as a point of comparison. In situ STM[34] and AFM[8] have shown a $\sqrt{3} \times \sqrt{3}$ structure which was initially misinterpreted as a simple hexagonal structure with 1/3 monolayer (ML) Cu coverage. On the other hand, ex situ electron diffraction and Auger electron spectroscopy studies[35] and electrochemical studies[3,36] suggested a model with a honeycomb lattice of Cu atoms (2/3 ML coverage) and sulfate/bisulfate anions adsorbed at the centers (1/3 ML coverage) above the Cu atomic plane. Recently, in situ X-ray scattering studies have shown that this structure is likely the correct model.[19]

During Hg UPD, it is likely that a similar honeycomb structure of coadsorption is formed, in particular, because the atomic ratio of Hg to sulfate/bisulfate anions is also 2:1. However, in the coadsorption structure shown in Figure 5(b), only lattice vector **b** matches the $\sqrt{3} \times \sqrt{3}$ structure. On the other hand, lattice vector **a** is compressed by 16% and rotated by 6.3° from the $\sqrt{3} \times \sqrt{3}$ direction. This was a bit surprising since the nearest-neighbor distance in bulk Hg (3.01 Å) is larger than that of Cu (2.56 Å). Therefore, the chemical state of Hg in the coadsorption structure must be quite different from that of Cu in the honeycomb structure to account for this smaller lattice.

One major difference in chemical properties between Hg and Cu is that Hg^{2+} ions can be readily reduced to stable dimeric ions Hg_2^{2+} while Cu^{2+} cannot. The Hg−Hg distance in Hg_2SO_4 is known to be 2.50 Å,[37] which is significantly smaller than the nearest-neighbor distance in frozen bulk Hg. If we

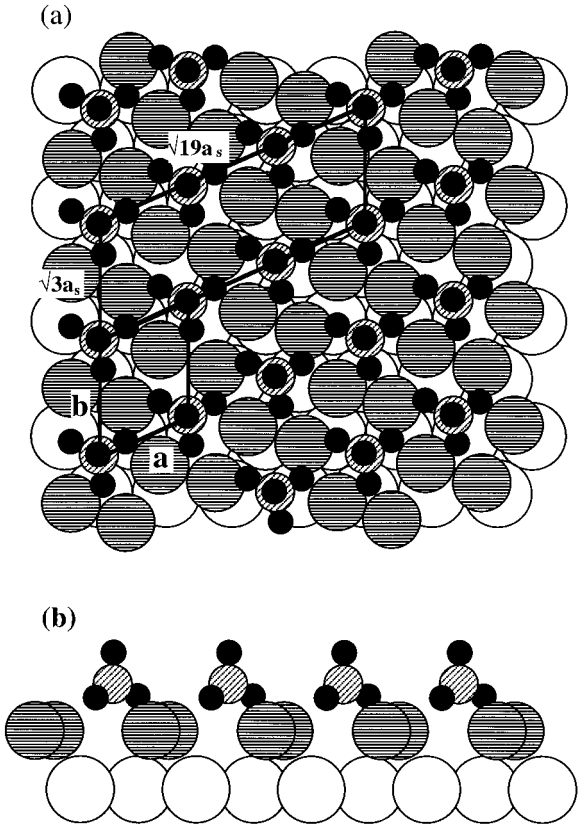

Figure 8. The distorted honeycomb structure of the coadsorbed Hg_2SO_4 overlayer at the first stage of Hg UPD where (a) is the top view and (b) is the side view along the *b* axis. The big open circles represent the Au atoms on the surface, and the hatched circles are the Hg atoms which form Hg_2^{2+} dimers aligned in the same direction. The sulfate anions are bonded above the hollow centers of the distorted honeycomb lattice.

assume that all the Hg_2^{2+} pairs are aligned in the direction about 18.3° from the nearest Au−Au direction, as shown in Figure 8(a), the one-dimensional compression can be readily explained. The open circles in Figure 8(a) represent the Au(111) substrate atoms, and the large hatched circles represent Hg atoms. The Hg atoms touching each other represent the Hg_2^{2+} pairs with a nearest Hg−Hg distance of 2.50 Å. With the structural model shown in Figure 8(a), the nearest Hg−Hg distance between two neighboring mercurous dimers can be calculated to be about 2.88 Å, which is only 4.3% smaller than the nearest Hg−Hg distance in bulk Hg. This slightly smaller size could be the effect of +1 charge on each Hg atoms of Hg_2^{2+} dimer. The small gray circles at the center of the hollow sites of the distorted honeycomb Hg lattice are sulfur atoms. The dark small circles are the oxygen atoms of sulfate/bisulfate anions, three of which are bonded to the Hg atoms below while the other one points up. The side view (Figure 8(b)) shows the cross section along **b**, which presents a bilayer structure along the surface normal. It is important to point out that the overlayer lattice size, geometry, and its orientation relative to the Au(111) substrate are precisely measured in our experiments. However, the exact registry of the Hg atoms on the Au(111) surface and how the oxygen atoms are bonded to the Hg adlayer are unknown so far. We are in the process of taking complete nonspecular crystal truncation rod measurements which, in principle, should provide more detailed information of the Hg atom registry on the Au(111) surface. On the other hand, EXAFS measurement might provide information about the local arrangement of oxygen and Hg atoms.

According to the above model, the net charge deposited per unit cell onto the surface is equivalent to either a Hg_2SO_4 or $Hg_2HSO_4^+$. We believe that the first UPD peak at $E = +0.93$ V in Figure 2 corresponds to a transition from sulfate/bisulfate adlayer to a Hg_2^{2+} adlayer coadsorbed with sulfate/bisulfate. The deposition of these coadsorbed species is a combination of the reorganization of the adsorbed sulfate/bisulfate anions and the deposition of more Hg ions and anions from the bulk solution. The net charge of the reduction peaks around +0.93 V is about 98 ± 10 μC cm^{-2}. Interestingly, the net charge transfer corresponding to the double-layer structural change from a 0.20 ML of SO_4^{2-} (Eden and Itaya's model) to a 0.375 ML of Hg_2SO_4 will have a net charge transfer of 89 μC cm^{-2} which matches well with the measured net charge transfer. On the other hand, the transition from a 0.40 ML of HSO_4^- to a 0.375 ML of $Hg_2HSO_4^+$ should give a net charge transfer of 172.2 μC cm^{-2}, which is much larger than the experimental value. If the faradaic current for reducing Hg^{2+} to Hg_2^{2+} is also to be included, the net charges of these two models are 256 and 339 μC cm^{-2}, respectively. These value are much larger than our experimental value and would indicate that little, if any, faradaic process is taking place. Taking into account that Hg_2^{2+} is always present in Hg^{2+} solutions (due to the equilibrium between both species), Hg_2SO_4 can be readily formed without a simultaneous redox reaction. Thus, Hg_2SO_4 is the most likely adsorbate species. The formation of Hg_2SO_4 also explains the high packing density and stability of the coadsorption structure which is not likely to be achieved by $Hg_2HSO_4^+$ due to strong coulombic repulsion. Further details will be given elsewhere,[38] together with a detailed study of the change of Hg UPD peaks with the concentration of Hg^{2+} and sulfate.

5. Conclusions

As a summary, we have found a highly ordered coadsorbed structure formed at the first stage of Hg UPD on Au(111) electrodes in 0.10 M H_2SO_4 containing 1.0 mM Hg^{2+} ions. This structure consists of a one-dimensional compressed honeycomb lattice of partially charged Hg atoms with honeycomb centers occupied by sulfate anions which are above the Hg plane. The compression of the lattice is likely due to the formation of mercurous (Hg_2^{2+}) ions which have a much shorter Hg−Hg distance than that in bulk Hg. The net charge transferred under the first Hg UPD peak suggests that the chemical state of the species in the coadsorbed structure is likely Hg_2SO_4. Our results indicate that both the chemical state of cations and the nature of anions are important in the resulting electrodeposited structures.

Acknowledgment. This work was supported by the Office of Naval Research and the National Science Foundation. Most synchrotron X-ray experiments were performed at Exxon beamline X10B at the National Synchrotron Light Source, Brookhaven National Laboratory, which is supported by the U.S. Department of Energy, Division of Materials Science and Division of Chemical Structures (DOE Contract No. DE-AC02-76CH0016). Preliminary X-ray measurements were also performed at the Cornell High Energy Synchrotron Source, which is supported by the National Science Foundation. We thank Dr. K. Liang for his generous technical help and scientific discussions. We also thank Dr. Enrique Herrero, Sean Smith, and Shaowei Chen for their participating in part of the experiments and for their helpful discussions.

References and Notes

(1) Gómez, R.; Yee, H. S.; Bommarito, G. M.; Feliu, J. M.; Abruña, H. D. *Surf. Sci.* **1995**, *335*, 101.
(2) Ye, H. S.; Abruña, H. D. *Langmuir* **1993**, *9*, 2460.
(3) Shi, Z.; Lipkowski, J. *J. Electroanal. Chem.* **1994**, *365*, 303.

(4) Borges, G. L.; Kanazawa, K. K.; Gordon, J. G.; Ashley, K.; Richer, J. *J. Electroanal. Chem.* **1994**, *364*, 289.

(5) Zelenay, P.; Rice-Jackson, L. M.; Wieckowski, A. *Surf. Sci.* **1991**, *256*, 253.

(6) Ogasawara, H.; Inukai, J.; Ito, M. *Surf. Sci.* **1994**, *311*, L665.

(7) Sashikata, K.; Furuya, N.; Itaya, K. *J. Electroanal. Chem.* **1991**, *316*, 361.

(8) Maanne, S.; Hansma, P. K.; Massie, J.; Elings, V. B.; Gewirth, A. A. *Science* **1991**, *251*, 183.

(9) Abruña, H. D. In *Advances in Chemical Physics*; Prigogine, I., Rice, S. A., Eds.; John Wiley & Sons: New York, NY, 1990; Vol. LXXVII, p 255.

(10) Toney, M.; McBreen, J. *Electrochem. Soc. Interface* **1993**, *2* (1), 22.

(11) Toney, M. F.; Ocko, B. M. *Synchrotron Radiation News* **1993**, *6* (5), 28.

(12) Schadewald, L. A. *J. Electrochem. Soc.*, **1984**, *131*, 1583.

(13) Sherwood, W. G.; Bruckenstein, S. *J. Electrochem. Soc.* **1978**, *125*, 1098.

(14) Sherwood, W. G.; Untereker, D. F.; Bruckenstein, S. *J. Electrochem. Soc.* **1978**, *125*, 384.

(15) Shay, M.; Bruckenstein, S. *Langmuir* **1989**, *5*, 280.

(16) Salie, G. *J. Electroanal. Chem.* **1989**, *259*, 315.

(17) Chen, C.-H.; Gewirth, A. A. *Phys. Rev. Lett.* **1992**, *68* (10), 1571.

(18) Inukai, J.; Sugita, S.; Itaya, K. *J. Electroanal. Chem.* **1996**, *403*, 159.

(19) Toney, M. F.; Howard, J. N.; Richer, J.; Borges, G. L.; Gordon, J. G.; Melroy, O. R.; Yee, D.; Sorensen, L. B. *Phys. Rev. Lett.* **1995**, *75* (42), 4472.

(20) Huckaby, D. A.; Blum, L. *J. Electroanal. Chem.* **1991**, *315*, 255. Blum, L.; Huckaby, D. A. *J. Electroanal. Chem.* **1994**, *375*, 69. Blum, L.; Huckaby, D. A.; Legault, M. *Electrochim. Acta*, in press.

(21) Magnussen, O. M.; Hageböck, J.; Hotlos, J.; Jürgen, R. *Faraday Discuss.* **1992**, *94*, 329.

(22) Edens, G. J.; Gao, X.; Weaver, M. J. *J. Electroanal. Chem.* **1994**, *375*, 357.

(23) Shi, Z.; Lipkowski, J.; Gamboa, M.; Zelenay, P.; Wieckowski, A. *J. Electroanal. Chem.* **1994**, *366*, 317.

(24) Fuoss, P. H.; Liang, K. S.; Eisenberger, P. In *Synchrotron Radiation Research: Advances in Surface and Interface Science*; Bachrach, R. Z., Ed.; Plenum: New York, 1982; Vol. 1.

(25) Robinson, I. K.; Tweet, D. J. *Rep. Prog. Phys.* **1992**, *55*, 599.

(26) Samant, M. G.; Toney, M. F.; Borges, G. L.; Blum, L.; Melroy, O. R. *Surf. Sci. Lett.* **1988**, *193*, L29. Ocko, B. M.; Wang, J.; Davenport, A.; Isaacs, H. *Phys. Rev. Lett.* **1990**, *65* (12), 1466.

(27) Wang, J.; Ocko, B. M.; Davenport, A. J.; Isaacs, H. S. *Phys. Rev. B* **1992**, *46*(16), 10321.

(28) Li, J.; Abruña, H. D. In preparation.

(29) (a) Li, J.; Liang, K. S.; Camellone, N., III; Leung, T. Y. B.; Scoles, G. *J. Chem. Phys.* **1995**, *102*, (12), 5012. (b) Li, J.; Liang, K. S.; Scoles, G.; Ulman, A. *Langmuir* **1995**, *11*, 4418.

(30) *International Tables for X-ray Crystallography*; Ibers, J. A., Hamilton, W. C., Eds.; Kynoch: Birmingham, 1974; Vol. IV.

(31) Gibbs, D.; Ocko, B. M.; Zehner, D. M.; Mochrie, S. G. J. *J. Phys. Rev. B* **1988**, *38*, 7303.

(32) Kolb, D. M.; Schneider, J. *Electrochim. Acta* **1986**, *31* (8), 929.

(33) Li, J.; Abruña, H. D. Unpublished.

(34) Magnussen, O. M.; Hotlos, J.; Nichols, R. J.; Kolb, D. M.; Behm, R. J. *Phys. Rev. Lett.* **1990**, *64*, 2929.

(35) Zei, M. S.; Qiao, G.; Lehmpfuhl, G.; Kolb, D. M. *Ber. Bunsen-Ges. Phys. Chem.* **1987**, *91*, 349.

(36) Shi, Z.; Lipkowski, J. *J. Electroanal. Chem.* **1994**, *364*, 289.

(37) Cotton, F. A.; Wilkinson, G. *Advanced Inorganic Chemistry*, 5th ed.; John Wiley & Sons: New York, 1988; p 508.

(38) Li, J.; Herrero, E.; Abruña, H. D. In preparation.